ORIGINAL RESEARCH ARTICLE

New Composition Based Technique for Solidification Cracking Resistance Evaluation

RAFAEL GIORJAO, BENJAMIN SUTTON, and ANTONIO RAMIREZ

Predicting the occurrence of solidification cracking during the solidification of metallic alloys by numerical simulation is a crucial move for avoiding such defects. Several models are widely available, however, the application of such are impacted due to the specific and not accessible parameters required. A simple, composition-based approach to rank solidification cracking susceptibility is presented. The procedure links computational thermodynamic and computational fluid dynamics (CFD) to provide an evaluation tool for solidification cracking. The method is related to the liquid filling phenomena in dendritic arms during solidification, which plays a critical role in solidification cracking phenomena. The dendritic profiles were constructed using the fraction of solid calculated by commercial thermodynamic software packages. The calculated results were compared with experimental solidification cracking data and showed satisfactory accuracy. The method capability to rank the solidification cracking propensity of similar alloys based on composition provides an important new operative tool to aid alloy development in welding and additive manufacturing related areas.

https://doi.org/10.1007/s11661-021-06244-2

I. INTRODUCTION

SOLIDIFICATION cracking occurs in metals when intergranular liquid films rupture within the semisolid region that forms as solidification progresses. Solidification shrinkage and thermal contraction act to separate solidifying grains that are disconnected by liquid films. If an insufficient amount of liquid is present to accommodate thermally induced strains within the semisolid network, solidification cracks can form.[1] In that way, the liquid's capability to fill between dendritic arms during solidification (backfilling) plays a critical role in solidification cracking resistance.

Often referred to as hot cracking or hot tearing in the literature, solidification cracks are commonly found during metals joining and manufacturing processes, *e.g.*, welding[2,3] and casting.[3,4] Solidification cracking issues have also been realized during the recent acceleration of metals additive manufacturing technologies.[5–7] The detection of solidification cracks immediately after processing results in costly rework or, in extreme cases, components must be discarded. If solidification cracks go undetected, the resulting service life of the component may be jeopardized.

RAFAEL GIORJAO, BENJAMIN SUTTON, and ANTONIO RAMIREZ are with the Welding Engineering, Department of Materials Science and Engineering, The Ohio State University, 1248 Arthur E Adams Dr, Columbus, OH 43221. Contact e-mail: ramirez.49@osu.edu

Manuscript submitted October 28, 2020, accepted March 1, 2021.

The conditions which lead to solidification crack formation can be quite complex. Broadly, these conditions can be mechanical or metallurgical in nature.[3,8] Mechanical contributions include conditions that lead to the development of stress and strain across a solidifying grain structure, *i.e.*, thermal contraction and restraint imposed by fixturing and/or section thickness. Metallurgical conditions are inherent to the solidifying alloy chemistry, *i.e.*, crystal structure of the solidifying grains, diffusivity in liquid and solid phases, liquid viscosity, surface tension, grain morphology/size, *etc.* Of course, many of these mechanical and metallurgical conditions exhibit spatial and temporal dependencies, making their behavior sensitive to the solidifying system's thermal energy distribution and heat extraction conditions.

There are many classical examples of alloy systems that exhibit a propensity to form solidification cracks during processing. Solidification crack formation is often associated with solute segregation and/or eutectic reactions at the latter stages of solidification. For example, solidification cracking can occur in austenitic stainless steels that exhibit A-mode solidification due to impurity (S and P) segregation.[9] The strong partitioning of impurity elements to the terminal liquid causes a local depression of the solidus temperature and increases the propensity for solidification crack formation. An example of eutectic reactions contributing to solidification cracking can be found in highly alloyed Ni-base materials, where the presence of carbide and/or topologically close-packed phase eutectic liquid during

Published online: 19 April 2021

terminal solidification can promote crack formation.[10–12] Many other examples can be found in the literature that addresses solidification cracking issues in other alloy systems, including aluminum alloys,[4,13] magnesium alloys,[14] low alloy steels,[15] high-Mn steels[16–18] and high entropy alloys.[19,20] The intent of listing these examples is not to provide an all-encompassing overview of material systems that exhibit solidification cracking issues but rather highlight the problem's wide-reaching nature.

Given the industrial significance of solidification cracking, various approaches have been developed to experimentally or computationally assess the solidification cracking susceptibility of materials. Experimental techniques generally rely on mechanically restraining a controlled solidification front to induce crack formation and assess causal factors. Examples include varying the chemical composition of the solidifying material and/or determining critical mechanical conditions that cause cracking.[4,21,22] Computational approaches to study solidification cracking have taken many forms to simulate various aspects of the solidification cracking problem.

Computational thermodynamic or coupled thermodynamic-kinetic models are often used to assess solute segregation, phase evolution, and solidus temperature depression that can act as indicators for solidification cracking behavior.[23–26] A common approach for this type of analysis is to use the Calphad method coupled with solidification models (such as those from Scheil,[27] Brody–Flemings,[28] or Clyne–Kurz[29]) to evaluate the non-equilibrium solidification temperature range (STR) of materials.

The Rappaz–Drezet–Gremaud (RDG) model was developed to describe solidification cracking behavior by considering solid deformation, shrinkage, and interdendritic liquid feeding within the mushy zone.[30] The RDG model predicts that solidification cracks will nucleate when the pressure of the interdendritic liquid flowing between neighboring dendrites drops below a critical value. The pressure drop condition originates from a competition between interdendritic fluid flow and the strains induced from the solid network's deformation and shrinkage. A void, which can serve as a solidification crack nucleation site, can form if the deformation and shrinkage contributions cause the interdendritic liquid pressure to drop below a certain cavitation pressure. The RDG model was used to evaluate solidification cracking susceptibility by considering the critical strain rate needed to induce cavitation.[30] The modeled solidification cracking tendencies for a series of Al-Cu alloys agreed with other studies.[30,31] The RDG model was originally developed to describe hot cracking observed in casting, however, it has been extended to solidification cracking observed during welding[32,33] and additive manufacturing.[20] However, the RDG model's application requires a set of complex alloy-dependent parameters that are not readily available for a wide range of materials.

Kou developed a cracking criterion that considers grain separation, grain growth into the liquid, and liquid feeding into the intergranular channel that forms between neighboring columnar dendrites during solidification.[34] Using Kou's approach, crack initiation is assumed to occur when the volumetric flow of liquid is unable to compensate for the net expansion of the intergranular space between the dendrites. An index was proposed where the steepness of a temperature (T) *vs* square root fraction solid $\left(f_s^{1/2}\right)$ curve, *i.e.* $\left|\mathrm{d}T/d\left(f_s^{1/2}\right)\right|$, near $f_s^{1/2}=1$ can be used to assess solidification cracking susceptibility, where higher steepness indicates higher susceptibility. The index is quite convenient given that Scheil simulations which model solid evolution during non-equilibrium solidification (often plotted as T *vs.* f_s) can easily be manipulated to reach the desired form. Furthermore, many commercially available computational thermodynamic software packages can readily perform Scheil solidification simulations.[35,36] Using the proposed steepness index, Kou demonstrated that $\left|\mathrm{d}T/d\left(f_s^{1/2}\right)\right|$ near $f_s^{1/2}=1$ correlated with experimental solidification cracking data of aluminum alloys from literature.[37] Kou later modified the cracking index to be the T *vs.* $f_s^{1/2}$ curve's maximum steepness rather than a somewhat arbitrary value near $f_s^{1/2}=1$.[37] The approach has also been modified for cases where solute back diffusion causes a deviation from Scheil behavior by using the solidification model of Clyne and Kurz to generate T *vs.* $f_s^{1/2}$ curves.[29,38,39]

A new approach to evaluate solidification cracking susceptibility has been developed that links computational thermodynamic and computational fluid dynamics (CFD). The proposed approach shares characteristics with the methodologies proposed by Rappaz[30] and Kou.[37,39] Like the RDG model, it covers columnar dendritic grains growing in one direction that are subjected to tensile deformation normal to the growth direction and liquid feeding opposite to the growth direction.[30] However, the new model does not require a large set of material parameters. Like the solidification cracking criterion of Kou, the approach focuses on events occurring at the grain boundary, including the separation of grains from tensile deformation, growth of grains due to solidification, and feeding of liquid along the intergranular channel between neighboring columnar dendrites.[37,39] The purpose of the present study is to present the new computational approach to rank composition regarding the solidification cracking susceptibility and test it against other solidification cracking metrics and experimental investigations from the literature.

II. METHODOLOGY

The proposed method is based on the backfilling phenomena, which consists on the drawing liquid through a dendritic network to feed solidification shrinkage. Solidification cracks are expected in systems that exhibit less backfilling: the harder a liquid metal fills the dendritic arms, the most cracking susceptibility is anticipated.

Two major phenomena are directly related to resisting solidification crack formation: lateral grain growth and liquid feeding along the grain boundary to resist cracking.[34] Therefore, the liquid feeding behavior, which is composition-dependent, can be used to compare similar alloy cracking susceptibilities.

This paper aims to use the flow resistance of liquid metal between neighboring dendrites to rank the solidification cracking susceptibility of similar alloys. Such flow resistance will be measured by the pressure difference between inlet and outlet of a calculated composition-based dendritic profile structure. By comparing the pressure difference (drop) values, such method will be capable of ranking the solidification cracking susceptibility of similar systems. The presented method will be referred as Flow Resistance Technique (FRT) in this paper.

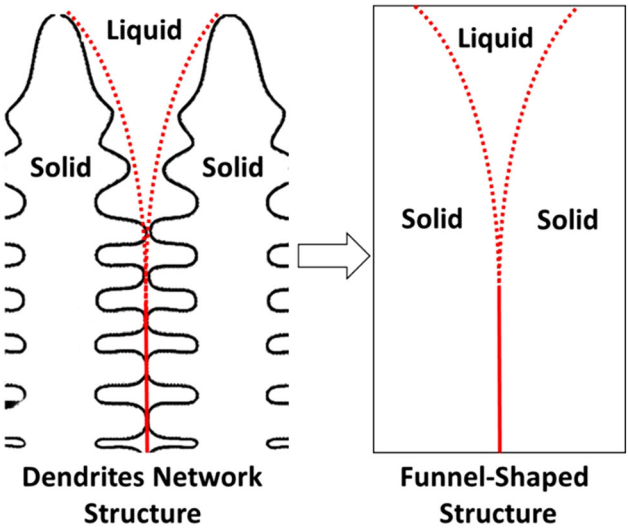

Fig. 1—Dendritic profile and funnel shaped approximation.

A. *The Pressure Drop Analysis*

In fluid dynamics, the Darcy–Weisbach equation relates the pressure drop due to friction along a given length of pipe to the average flow velocity for an incompressible fluid. The relationship is expressed as:

$$\Delta p = f_D \cdot L \cdot \frac{\rho}{2} \cdot \frac{\langle v \rangle^2}{D} \quad [1]$$

Δp is the pressure drop, f_D is the friction factor, $L$is the pipe length, ρ is the liquid density, v is the liquid velocity, and D is the pipe diameter. For laminar flow, the friction factor is inversely proportional to the Reynolds number ($f_D = 64/\mathrm{Re}$). Making this substitution, the Darcy–Weisbach equation is rewritten as Eq. [2]:

$$\Delta p = 128 \cdot \pi \cdot L \cdot \frac{\mu Q}{D^4} \quad [2]$$

Q is the volumetric flow rate (proportional to v) and μ is the liquid dynamic viscosity. $Q(v)$ and L, as discussed in the next sections, will be constant for the same alloy system. In that way, Eq. [2] reduces to:

$$\Delta p = f\left(\frac{\mu}{D}\right) \quad [3]$$

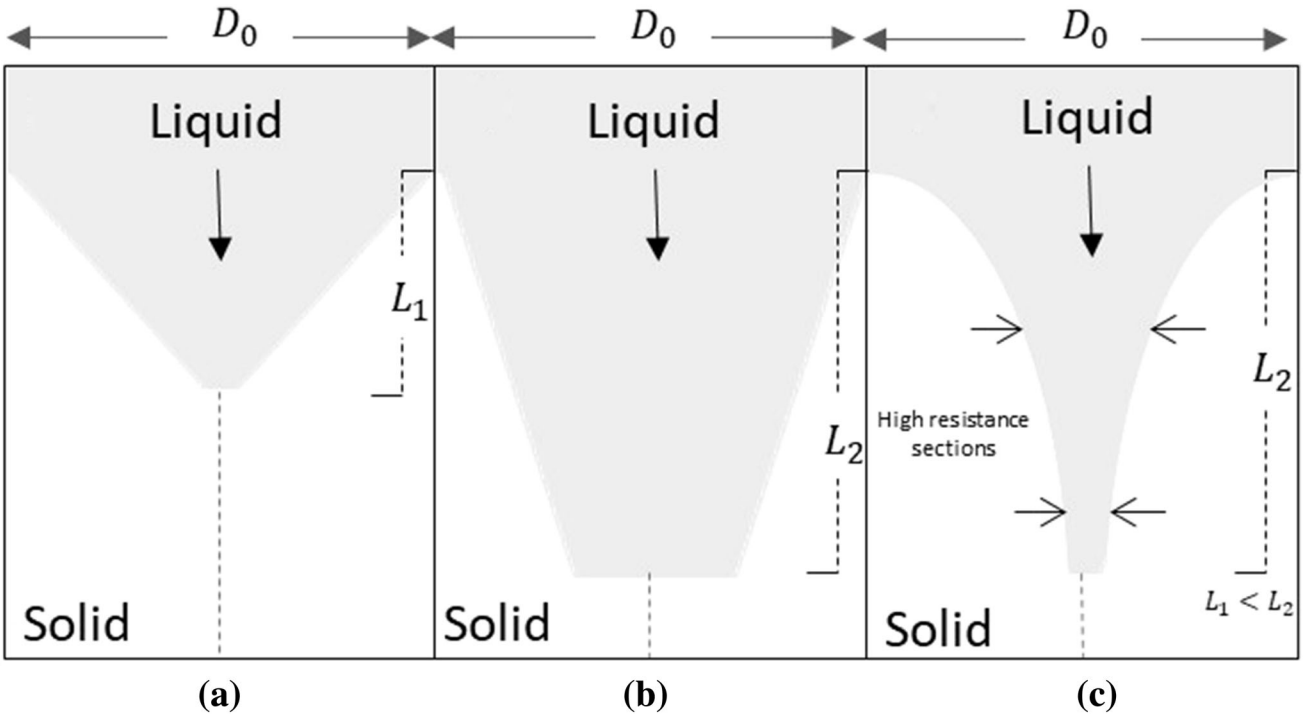

Fig. 2—Hypothetical funnel-shaped structures fluid flow resistance comparison. Fluid resistance order: (*a*) < (*b*) < (*c*).

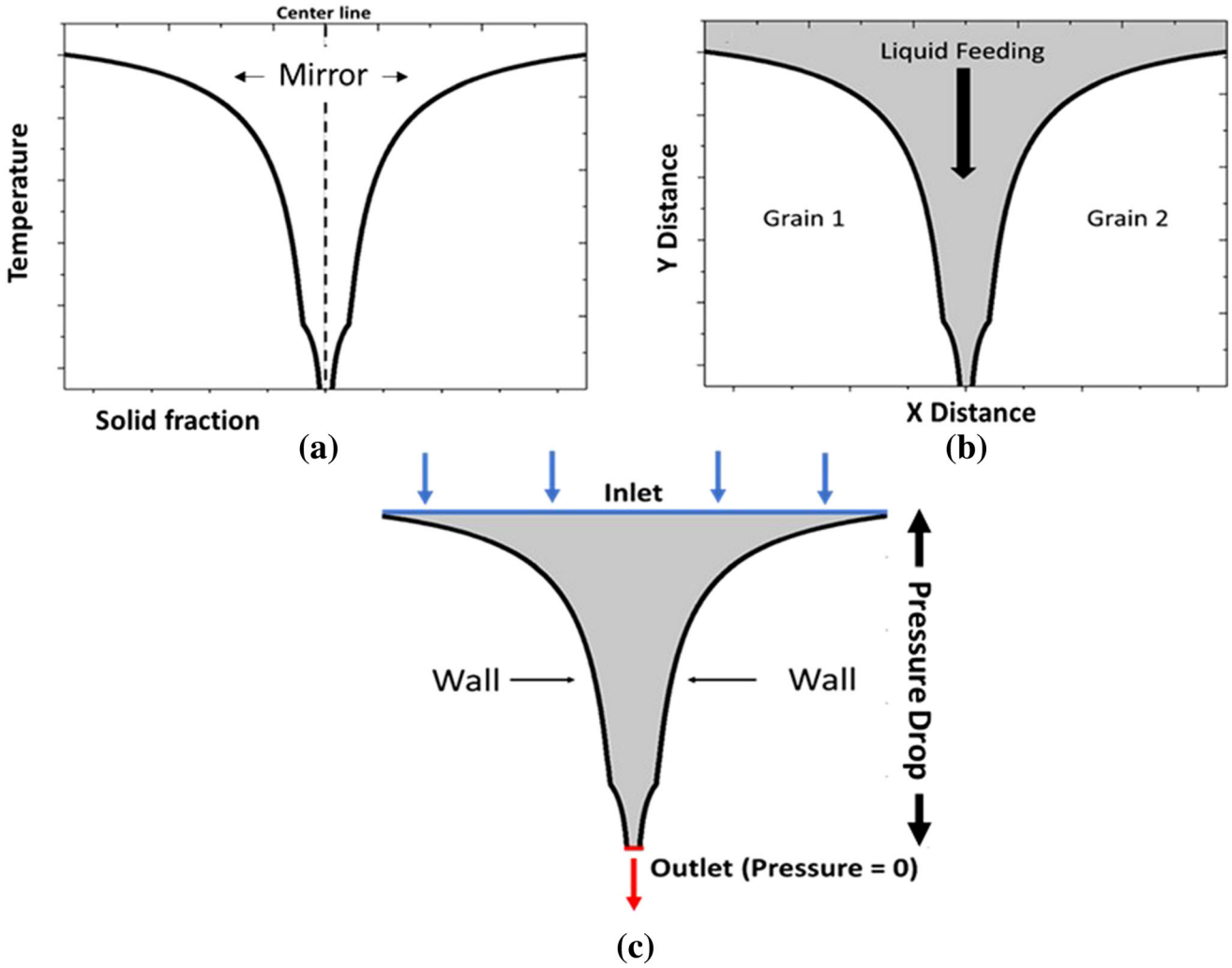

Fig. 3—(*a*) Mirrored Scheil diagram, (*b*) liquid feeding model, (*c*) Inlet and outlet schematics.

The interdendritic gap between neighboring dendrites will be treated as the pipe diameter (D), as seen in Figure 1. Dynamic viscosity will be calculated for each composition using a Calphad approach.

To illustrate the methodology, three different hypothetical funnel-shaped structures are presented in Figure 2. By comparing the pressure drop of the three conditions, the fluid's resistance through the funnel can be ranked as $(c) > (b) > (a)$. First, the greater the funnel length, the greater is the resistance experienced by the liquid. Second, and more critical for the presented work, is the funnel wall geometry. Section reductions can promote different responses in the fluid flow. Metallurgically, such funnel sections can be related to the metal solidification front. Materials solidification structures/sequences that facilitate the fluid flow, such as (*a*) or (*b*), present higher solidification cracking resistance.

A metal composition capable of reducing the overall solidification temperature range and/or offering favorable backfilling conditions (low resistance sections) can minimize solidification cracking. Liu *et al.*[40] observed that different Cr additions in Co-Al-W based superalloys promoted different responses in solidification cracking resistance. The increase in cracking resistance with Cr additions was attributed to narrowing the solidification temperature range and increasing the level of liquid to backfill cracks.

The pressure drop concept was already explored by Rappaz *et al.* in the RDG model.[30] The RDG model estimates the interdendritic liquid pressure drop at the dendrite base due to insufficient liquid feeding to compensate for solidification shrinkage and thermal contraction. The present model aims to implement a CFD approach to circumvent the need for certain parameters listed by the RDG model (*i.e.*, shrinkage factor), providing a simplified tool to rank alloys according to their cracking susceptibility.

The present technique evaluates only solidification crack initiation and does not account for propagation. For the steady-state conditions considered, the requirement for a crack to initiate and propagate are the same unless an increase in deformation is observed.[30]

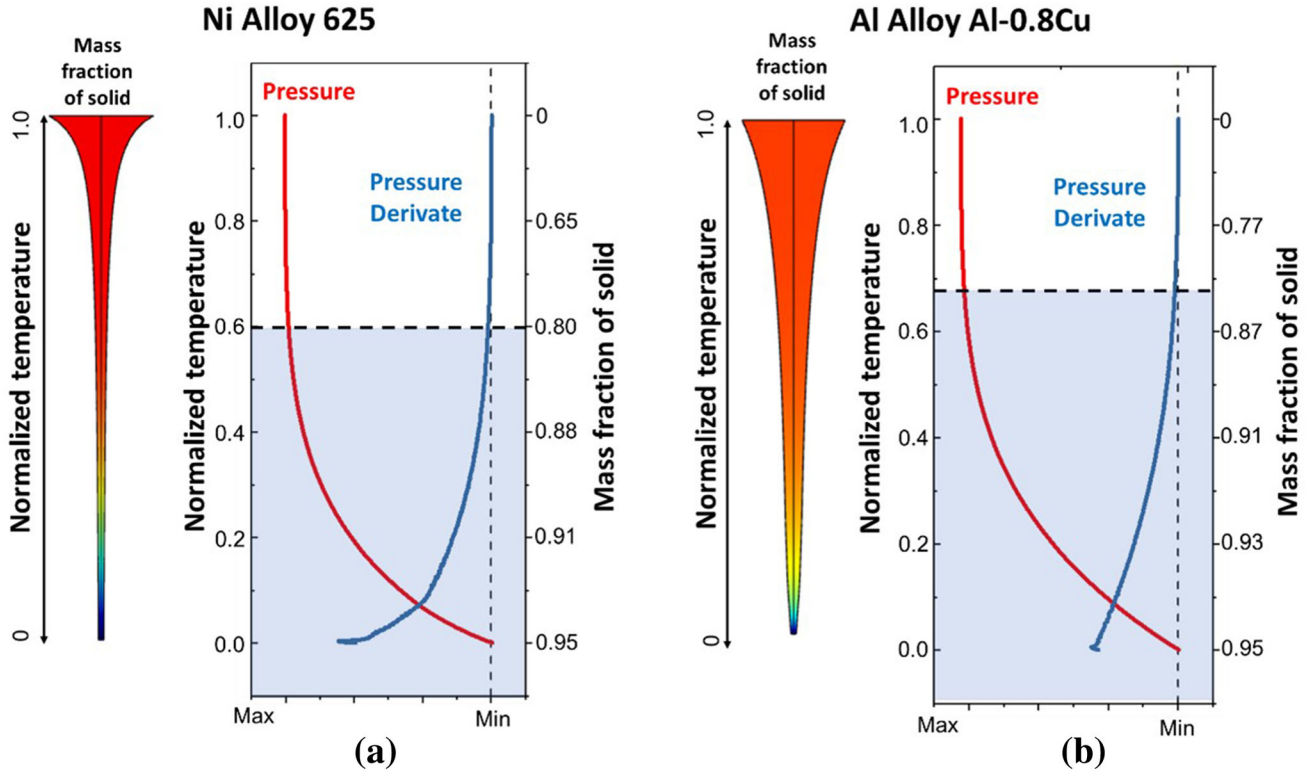

Fig. 4—Pressure and pressure derivate analysis for (*a*) Ni alloy 625 and (*b*) Al alloy Al-0.8Cu.

B. *The Dendritic Profile*

As proposed by Kou *et al.*[34] and Rappaz *et al.*,[30] the solid/liquid interface can be approximated by a function of the solid fraction (f_s)during solidification. For example, Kou *et al.*[34] considered that $(f_s)^{1/2}$ curves near $(f_s)^{1/2} = 1$ were a good approximation for the solid/liquid interface and for the RDG model Rappaz *et al.*[30] considered just (f_s) to represent the solid/fraction interface. A similar approach was applied in this work, where solid fraction f_s from Scheil solidification simulation results were used to approximate the solid/liquid interface morphology. The interface morphology was constructed by considering the solid/liquid interface temperature as a function of solid fraction. All Scheil simulations were carried out using ThermoCalc 2020a.[36] The same solid fraction range must be considered to compare the solidification cracking behavior of different alloy compositions. This range should be related to the highest cracking susceptibility region during solidification. Working with Al-Cu alloys, Guven *et al.*[41] have shown that solidification cracking should happen when the solid fraction reaches 0.96. Lu *et al.*[42] have shown similar results in Al-Si, where the critical solid fraction for solidification crack initiation should occur at the end of solidification but not above 0.96. Clyne and Davies[31] analysis selected 0.99 solid fraction. Kou[37] considered that grain boundary liquid films do not contribute to solidification cracking behavior at solid fraction values greater than 0.98. A solid fraction range between 0.95 and 0.98 range is commonly used by other investigators for determining the solidification temperature range and/or fraction eutectic.[11,30,43] It is recognized that a critical solid fraction for solidification cracking is not universal and is likely alloy-dependant.

In this paper, Scheil simulations with an endpoint of 0.95 solid fraction were considered. All solid fraction calculations were perform using the commercial thermodynamic software package ThermoCalc 2020a with the following databases, depending on the alloy of interest: Ni database TCNI9, Al database TCAL6, and steel/Fe database TCFE10.

C. *Simulation Set-Up*

Two $T(f_s)$ curves were put side-to-side to simulate the dendritic network, as shown in Figure 3(a). The temperature T was set proportional to the Y distance (height) and the solid fraction f_s was set proportional to the X distance.

The profiles were then imported in the COMSOL V5.4 software. Using CFD, a condition of steady-state liquid flow was established between the upper and bottom parts of the dendritic profile, as shown in Figure 3(b). An inlet condition was applied on the upper surface, and an outlet condition with a pressure value of 0 was applied on the bottom surface. The model does not require a specific flow rate, as long as the same value is applied in each study case (Eqs. [1] and [2]). In that case, an arbitrary constant flow velocity of 100 mm/min (4 in/min) in the inlet was assumed for every simulation.

Dynamic viscosity (μ) was the only material properties set on the model. Such property was calculated in

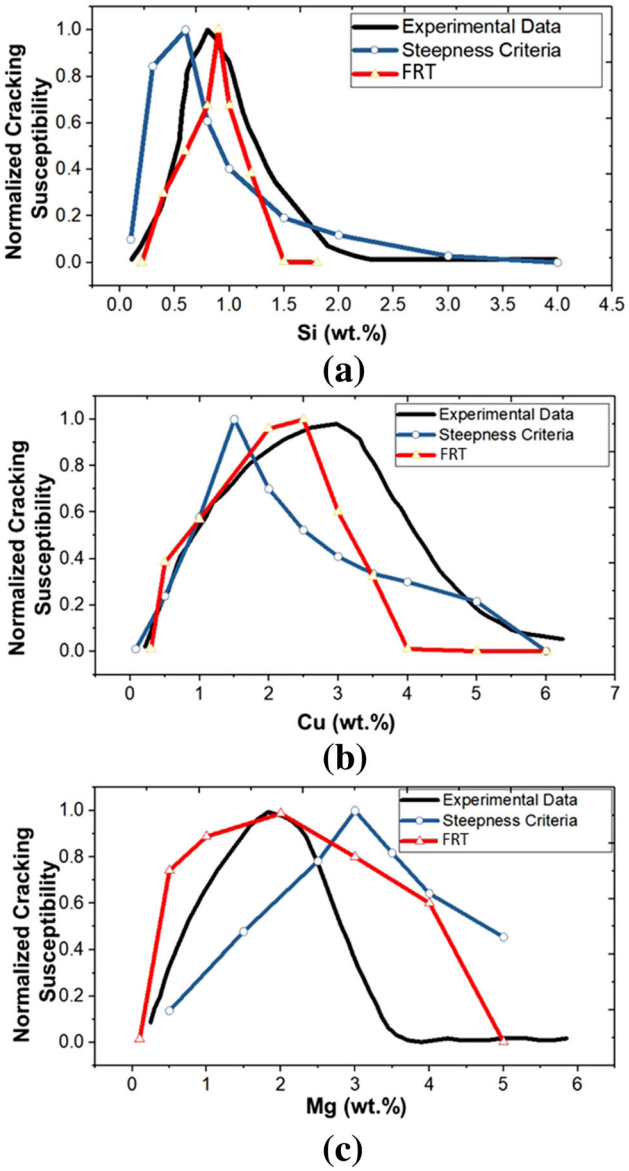

Fig. 5—Comparison between the maximum crack susceptibility from the present model (FRT), Kou's steepness criteria,[34] and experimental data for the (*a*) Al-Si,[44] (*b*) Al-Cu,[45] and (*c*) Al-Mg[46] binary systems. The data were normalized for comparison proposes.

ThermoCalc 2020a based on alloy composition and temperature.

Flow resistance was determined by calculating the pressure difference between the inlet and outlet of the simulated solidification profile, as shown in Figure 3(c). The higher the pressure difference, the higher is the resistance, and more cracking susceptibility is expected. It is projected that flow resistance (quantified by the calculated pressure difference) scales with solidification cracking susceptibility when comparing alloys.

According to the literature,[30,31,34,41] solidification cracking occurs during the terminal stage of solidification. In that way, a limited solid fraction range was considered to minimize computational time. As shown in Figure 4(a) for the Ni alloy 625 and Figure 4(b) for Al-0.8Cu, the pressure across the simulated solidification profile remains relatively constant until the later stages of solidification. The pressure begins to change at approximately 0.8 and 0.85 solid fraction for alloy 625 and Al-0.8Cu, respectively. Additional simulation trials were conducted with a variety of alloy systems to define a suitable minimum solid fraction for analysis. The lower solid fraction limit, which bounded the pressure drop, ranged between 0.78 and 0.85 across the systems evaluated. A lower solid fraction limit was defined at 0.8 for consistency within this investigation. Therefore, the solidification range for all subsequent simulations was bounded between 0.8 and 0.95 solid fraction.

III. RESULTS

In this paper, experimental solidification cracking evaluation techniques, such as transvarestraint test and cast pin tear test (CPTT) found in the literature, were used as a reference to assess the present model's reliability.

The transvarestraint test is widely applicable to most materials, and the results are quantitative, allowing relative susceptibility to solidification cracking to be easily determined. An autogenous weld is made across the sample as a downward bending motion is initiated by applying force at the loading rollers, which forces the sample to conform to the radius of the die block.

The cast pin tear test (CPTT) is a self-restrained solidification cracking test in which a material is cast in a copper mold and solidifies as a restrained pin. In the solidifying cast pin, thermal tensile strain is generated simultaneously from liquid–solid and solid-state shrinkage in the tested alloy and the copper mold's thermal expansion. That tensile strain is concentrated in the last portion of solidifying metal. Solidification cracking occurs when the tensile strain exceeds the material's inherent ductility in the solidification temperature range.[16]

All experimental and calculated susceptibility data presented in the next sections were normalized to facilitate the comparison. It is also important to state that experimental reference data comes from distinct procedures and authors; thus, some discrepancies are expected compared to the model results.

A. *Crack Susceptibility of Binary Al Alloys*

Cracking susceptibility curves have been developed for Al alloys that illustrate the cracking susceptibility behavior according to the alloy content. As the alloy content increases, cracking susceptibility initially increases to a peak value and decreases due to a crack healing effect.[2,13] The difference in the cracking susceptibility peak location in these different Al-based systems is associated with the fraction of eutectic liquid present at the end of solidification for a given composition. At the peak, the liquid completely wets the solidification grain boundary and promotes cracking. At compositions beyond the peak, the eutectic liquid has a backfilling, or crack healing, effect.[2,13]

The FRT was applied to find the most solidification cracking susceptible compositions of the binary Al-Si, Al-Cu, and Al-Mg, as presented in Figure 5. Kou's [34]

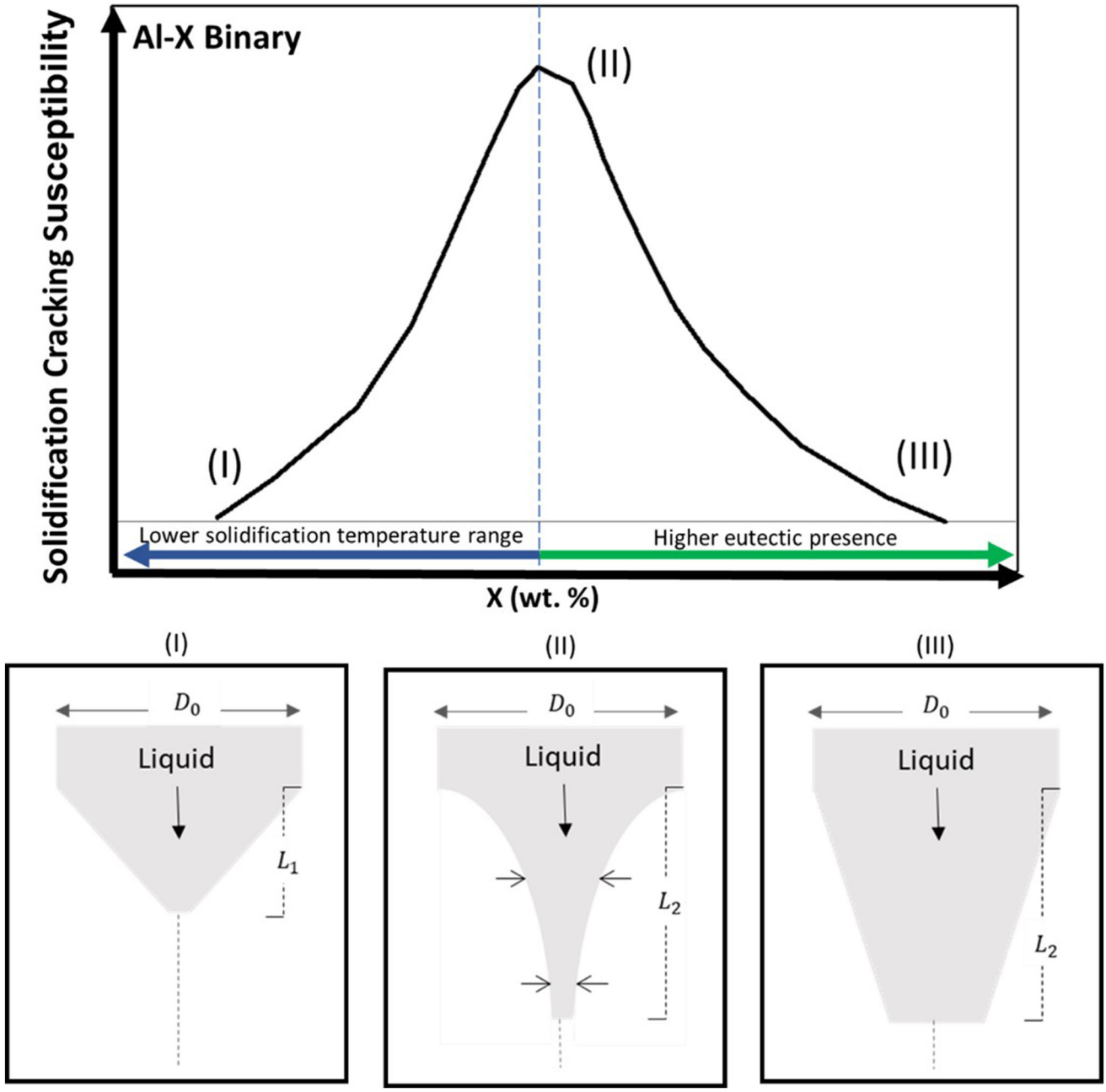

Fig. 6—Solidification cracking susceptibility for a hypothetical Al-X alloy and its correlation on FRT.

steepness criteria and experimental cracking susceptibility data from the literature were also compared to the FRT results. A peak cracking susceptibility at about 0.8 wt pct Si was reported by Singer *et al.*[44] in casting Al-Si alloys. Pumphrey and Lyons[45] observed a peak cracking susceptibility at 3 wt pct in Al-Cu alloys during solidification cracking experiments. In Al-Mg alloys, Dowd *et al.*[46] reported a peak cracking susceptibility at about 1.5 wt pct Mg during arc welding.

The FRT was able to capture the solidification cracking response in the binary Al systems. The model reproduces the typical-shaped profile and provides a good approximation for the peak cracking compositions. Peak solidification cracking susceptibility using the FRT was found to be 0.9 wt pct for Al-Si, 2.5 wt pct for Al-Cu, and 2 wt pct for Al-Mg. Kou's steepness criteria was also able to predict the ˆ shape curves, but the peak was slightly different from the experimental results.

As observed in the evaluated binary Al alloys, the FRT is capable of ranking alloys based on the balance between the solidification temperature range and the eutectic presence for each composition. Figure 6 illustrates the cracking susceptibility behavior for a hypothetical Al-X binary alloy and the model representation for each condition.

As the amount of the element X reduces, the solidification temperature range decreases as the system approaches the pure Al composition (*I*). Such a scenario

Alloy #	C	Si	Mn	Ni	Cr	Mo	Nb	S	P
1	0.017	0.27	0.58	30.4	4.0			0.0012	0.0113
2	0.006	0.58	1.2	27.8	14.4			0.0017	0.0276
3	0.01	0.57	1.18	20.2	20.4			0.0018	0.0274
4	0.018	0.24	1.32	16.9	14.3	0.01	0.43	0.0017	0.0161

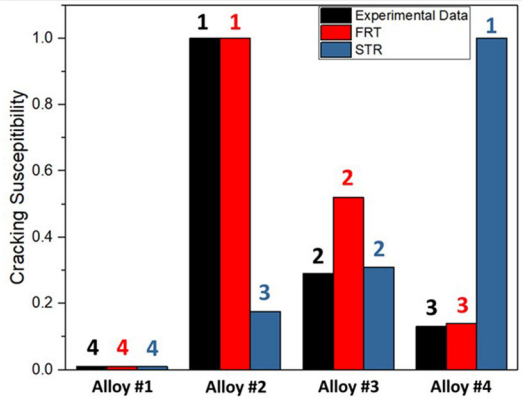

Fig. 7—Experimental transvarestraint test results for austenitic stainless steels[47] compared to the Flow Resistance Technique (FRT) and Solidification Temperature Range (STR). All calculated results were normalized for comparison proposes. Number on the top of the columns indicate the solidification cracking susceptibility rank for each technique.

Alloy #	Ni	Cr	Fe	Nb	Mo	C
690	60.51	29.45	9.13	-	-	0.029

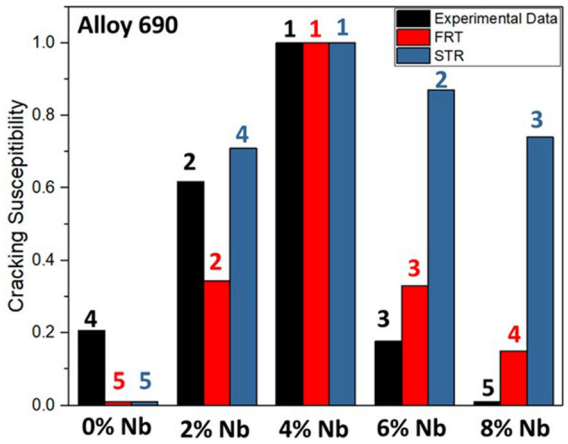

Fig. 8—Experimental CPTT test results for alloy 690[12] compared to the Flow Resistance Technique (FRT) and Solidification Temperature Range (STR). All results were normalized for comparison proposes. Number on the top of the columns indicate the solidification cracking susceptibility order for each technique.

shows faster growth of grains toward each other to bond together, thus lower conditions to cracks being formed. For higher X content, the system provides higher eutectic at the end of solidification. Such eutectic phases can heal the gaps between grains, avoiding the crack opening promoted by stresses. Similar behavior is also observed in a broader range of material classes, such as Ni-alloys.[11,23] Region (II) sums both long solidification

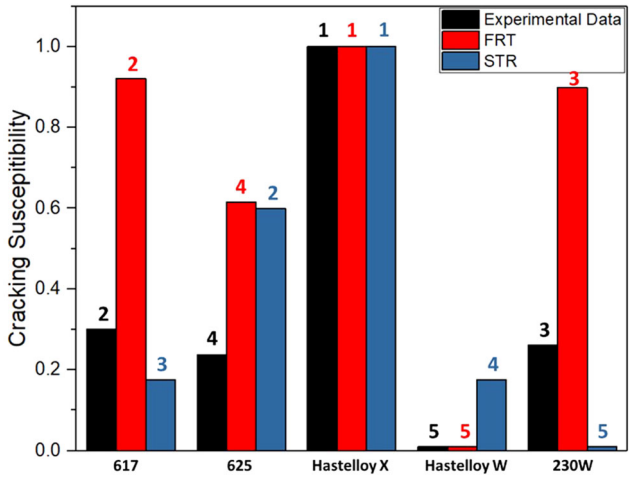

Fig. 9—Experimental transvarestraint test results for Ni-Based alloys[23] at 0.5 pct strain compared to the Flow Resistance Technique (FRT) and Solidification Temperature Range (STR). All calculated results were normalized for comparison proposes. Number on the top of the columns indicate the solidification cracking susceptibility rank for each technique.

temperature range and lack of sufficient eutectic phase, contributing to maximum cracking susceptibility.

B. *Crack Susceptibility of Austenitic Stainless Steels*

The chemical composition's influence on the weld solidification cracking susceptibility of austenitic stainless steels was investigated by Kadoi *et al.*[47] The laser transvarestraint test was performed to evaluate solidification cracking susceptibility. A high-speed camera was set up vertically to the center of the specimen to monitor the molten pool's geometry when the strain was applied. As seen in Figure 7, the FRT could rank the selected alloys in agreement with the experimental results (Maximum Crack Length). The model was able to get both effects of equivalent Cr and Ni. The addition of niobium increased the STR significantly, suggesting higher solidification cracking probabilities; however, it was not observed in both experimental and FRT results. As mentioned, STR only accounts for the temperature gap between solidus and liquidus and does not consider how the solid front evolves along with solidification, resulting in some disparity results, as observed.

C. *Crack Susceptibility of Ni Alloys*

Wheeling and Lippold *et al.*[12] explored Nb alloying effect on the solidification cracking susceptibility of Ni-based weld metals. In Figure 8, results from cast pin tear tests were compared to the calculated method to determine the effect of variable Nb content on the solidification cracking susceptibility of Alloy 690 (Ni-30Cr) filler metals.

Figure 8 shows the FRT predicted a cracking susceptibility peak at 4 wt pct Nb, the same observed in the experimental results. The FRT was also capable of capturing a similar trend observed in the cast pin test results, with more precision than STR. However, the

technique could not replicate the same least susceptible compositions. Such discrepancies are expected due to the varied nature of experimental references.

The present FRT was also used on Ni-based alloys with a greater composition variation. The selected alloys were 617, 625, Hastelloy X, Hastelloy W, and 230W. Transvarestraint maximum cracking distance (MCD) data was used as an experimental reference.[23]

Special care was taken to select the transvarestraint data in Ni alloys. For example, alloy 625 usually performs poorly at saturated strains during the transvarestraint test.[23] In actual practice, alloy 625 shows good resistance to weld solidification cracking and is often selected for use in moderate restraint applications to avoid problems with cracking, particularly when welding dissimilar materials.[48] When restraint is low, this liquid is available to heal any cracks that form by a backfilling mechanism, reducing the alloy 625 cracking susceptibility.

According to Figure 9, the FRT could correctly rank the alloys' solidification cracking behavior at 0.5 pct strain. The best fit was found using the lowest applied strain available when liquid is available to support the backfilling mechanism. As mentioned, the discrepancies observed are related to particularities of each experimental technique used as a reference. For example, the evaluated materials are also susceptible to ductility dip cracking (DDC); some portion of the crack length measured in the Varestraint test may be DDC extension off the solidification crack.[23]

IV. CONCLUSIONS

A new solidification cracking tecnique based on alloy composition was presented. The proposed flow resistance technique (FRT) is related to the backfilling phenomena that refer to drawing liquid back through a dendritic network to feed solidification shrinkage. This paper uses a combination of computational fluid dynamics and Calphad analysis to evaluate the dendritic network's flow resistance for different alloy compositions. The calculated solidification cracking susceptibility through the FRT was compared to experimental solidification cracking data from the literature. The following conclusions were made:

1. The FRT was able to capture the effect of alloying elements on the cracking susceptibility of binary Al systems and rank their cracking susceptibility following the same tendency demonstrated in experimental results.
2. The FRT captured the influence of composition variations on the weld solidification cracking susceptibility of fully austenitic stainless steels.
3. Evaluating the Ni-Nb system, the FRT was able to match the maximum cracking susceptibility composition found during cast pin tear testing. However, the method was not able to identify the composition with the lowest cracking susceptibility.
4. The FRT correlated well with transvarestraint data from Ni-based metals using the lowest applied strain available.
5. Discrepancies between experimental and the model results were observed. Such an outcome is due to the varied nature of experimental references.
6. The FRT model provides a fast methodology to computationally assess the solidification cracking susceptibility of alloys based on their composition. Such an approach can be used for material design, optimization, and selection for welding and additive manufacturing-related areas.

REFERENCES

1. J. Campbell: *Castings Practice*, Elsevier, Amsterdam, 2004.
2. S. Kou: *JOM*, 2003, vol. 55, pp. 37–42.
3. N. Coniglio and C.E. Cross: *Int. Mater. Rev.*, 2013, vol. 58, pp. 375–97.
4. D.G. Eskin, Suyitno, and L. Katgerman: *Prog. Mater. Sci.*, 2004, vol. 49, pp. 629–11.
5. D. Wang, Z. Wang, K. Li, J. Ma, W. Liu, and Z. Shen: *Mater. Des.*, 2019, vol. 162, pp. 384–93.
6. L.N. Carter, M.M. Attallah, and R.C. Reed: *Superalloys*, Wiley, Hoboken, 2012, pp. 577–86.
7. A. Hariharan, L. Lu, J. Risse, A. Kostka, B. Gault, E.A. Jägle, and D. Raabe: *Phys. Rev. Mater.*, 2019, vol. 3, art. no. 123602.
8. C.E. Cross: *Hot Cracking Phenomena in Welds*, Springer, Berlin, 2005, pp. 3–18.
9. V. Kujanpaa, N. Suutala, T. Takalo, and T. Moisio: *Weld. Res. Int.*, 1979, vol. 9 (2), pp. 55–75.
10. J.N. DuPont, M.R. Notis, A.R. Marder, C.V. Robino, and J.R. Michael: *Metall. Mater. Trans. A*, 1998, vol. 29A, pp. 2785–96.
11. B.T. Alexandrov, A.T. Hope, J.W. Sowards, J.C. Lippold, and S. McCracken: *Weld. World*, 2011, vol. 55, pp. 65–76.
12. R. Wheeling and J. Lippold: *Weld. J.*, 2016, vol. 95 (7), pp. 229–38.
13. S. Kou, V. Firouzdor, and I.W. Haygood: *Hot Cracking Phenomena in Welds III*, Springer, Berlin, 2011, pp. 3–23.
14. G. Cao and S. Kou: *Metall. Mater. Trans. A*, 2006, vol. 37A, pp. 3647–63.
15. V. Shankar and J.H. Devletian: *Sci. Technol. Weld. Join.*, 2005, vol. 10, pp. 236–43.
16. B.J. Sutton and J.C. Lippold: *Proc. Int. Offshore Polar Eng. Conf.*, 2013, vol. 9, pp. 340–47.
17. J. Yoo, K. Han, Y. Park, J. Choi, and C. Lee: *Sci. Technol. Weld. Join.*, 2014, vol. 19, pp. 514–20.
18. J. Yoo, B. Kim, Y. Park, and C. Lee: *J. Mater. Sci.*, 2015, vol. 50, pp. 279–86.
19. A.C. Martin, J.P. Oliveira, and C. Fink: *Metall. Mater. Trans. A*, 2020, vol. 51A, pp. 778–87.
20. Z. Sun, X.P. Tan, M. Descoins, D. Mangelinck, S.B. Tor, and C.S. Lim: *Scr. Mater.*, 2019, vol. 168, pp. 129–33.
21. T. Kannengiesser and T. Boellinghaus: *Weld. World*, 2014, vol. 58, pp. 397–21.
22. Suyitno, W.H. Kool, and L. Katgerman: *Metall. Mater. Trans. A*, 2004, vol. 35A, pp. 2917–26.
23. J.C. Lippold, J.W. Sowards, G.M. Murray, B.T. Alexandrov, and A.J. Ramirez: *Hot Crack. Phenom. Welds*, 2008, vol. II, pp. 147–70.
24. W. Rindler, E. Kozeschnik, and B. Buchmayr: *Steel Res.*, 2000, vol. 71, pp. 460–65.
25. J.N. DuPont: *Hot Cracking Phenomena in Welds III*, Springer, Berlin, 2011, pp. 265–93.
26. J. Draxler, J. Edberg, J. Andersson, and L.-E. Lindgren: *Weld. World*, 2019, vol. 63, pp. 1503–19.
27. E. Scheil: *Zeitschrift für Met.*, 1942, vol. 34, pp. 70–2.
28. M.C. Brody and H.D. Flemings: *Trans. Metall. Soc. Aime*, 1966, vol. 236 (5), pp. 615–24.

29. T.W. Clyne, M. Wolf, and W. Kurz: *Metall. Trans. B*, 1982, vol. 13B, pp. 259–66.
30. M. Rappaz, J.M. Drezet, and M. Gremaud: *Metall. Mater. Trans. A*, 1999, vol. 30A, pp. 449–55.
31. T.W. Clyne and G.J. Davies: *Br. Foundrym.*, 1981, vol. 74, pp. 65–73.
32. J.M. Drezet and D. Allehaux: *Hot Cracking Phenomena in Welds II*, Springer, Berlin pp, 2008, pp. 27–45.
33. C.E. Cross, N. Coniglio, P. Schempp, and M. Mousavi: *Hot Cracking Phenomena in Welds III*, Springer, Berlin, 2011, pp. 25–41.
34. S. Kou: *Acta Mater.*, 2015, vol. 88, pp. 366–74.
35. S.L. Chen, S. Daniel, F. Zhang, Y.A. Chang, X.Y. Yan, F.Y. Xie, R. Schmid-Fetzer, and W.A. Oates: *Calphad Comput. Coupling Phase Diagr. Thermochem.*, 2002, vol. 26, pp. 175–88.
36. J.O. Andersson, T. Helander, L. Höglund, P. Shi, and B. Sundman: *Calphad Comput. Coupling Phase Diagr. Thermochem.*, 2002, vol. 26, pp. 273–312.
37. S. Kou: *Weld. J.*, 2015, vol. 94, pp. 374s–388s.
38. K. Liu and S. Kou: *Sci. Technol. Weld. Join.*, DOI:10.1080/13621718.2019.1681160.
39. J. Liu and S. Kou: *Acta Mater.*, 2015, vol. 100, pp. 359–68.
40. C. Liu, Y. Sun, M. Wen, T. He, and J. Yu: *J. Manuf. Process.*, 2020, vol. 56, pp. 820–29.
41. Y.F. Guven, J.D. Hunt, B.Y.F. Guven, and J.D. Hunt: *Cast Met.*, https://doi.org/10.1080/09534962.1988.11818955.
42. L. Lu, A.K. Dahle, C. Davidson, and D. StJohn: *TMS Light Met.*, 2007, pp. 721–6.
43. J.N. Dupont, C.V. Robino, and A.R. Marder: *Acta Mater.*, 1998, vol. 46, pp. 4781–90.
44. A. Singer and P. Jennings: *J. Inst. Met.*, 1946, vol. 73, pp. 197–212.
45. W.I. Pumphrey and J.V. Lyons: *J. Inst. Met.*, 1948, vol. 74, pp. 439–55.
46. J.D. Dowd: *Weld. J.*, 1952, vol. 31 (10), pp. 448S–456S.
47. K. Kadoi and K. Shinozaki: *Metall. Mater. Trans. A*, 2017, vol. 48A, pp. 5860–69.
48. J.N. DuPont, J.C. Lippold, and S.D. Kiser: *Welding Metallurgy and Weldability of Nickel-Base Alloys*, Wiley, Hoboken, 2009.